Distributed neural computation and the evolution of the first brains

Vikram Chandra[1,2]*, Mehrana R. Nejad[3,4], Allison P. Kann[1,2], Ananya Salem[1,2], Karl A.P. Hill[1,2,5], L. Mahadevan[1,3,4], Mansi Srivastava[1,2]*

1. Department of Organismic and Evolutionary Biology, Harvard University, Cambridge MA 02138
2. Museum of Comparative Zoology, Harvard University, Cambridge MA 02138
3. School of Engineering and Applied Sciences, Harvard University, Cambridge MA 02138
4. Department of Physics, Harvard University, Cambridge MA 02138
5. Current address: Department of Biology, University of North Carolina at Chapel Hill, Chapel Hill NC 27599

* Corresponding Authors: vchandra1@fas.harvard.edu, mansi@oeb.harvard.edu

Abstract

Brains likely evolved from diffuse nerve nets in the Precambrian, but we do not know what the first brains looked like or how they were organized. Acoel worms, the sister lineage to all other animals with brains, offer a window into this transition. We studied the three-banded panther worm *Hofstenia miamia*, whose brain is diffuse and unlike any previously described: it shows little anatomical or functional regionalization or stereotypy. Worms forage successfully even after large portions of the brain are removed, suggesting most regions can perform most computations. Neural cell type markers are also distributed across the brain with little regionalization. High-resolution studies of hunting reveal that more brain tissue improves performance, but no specific brain region is required. These results lead us to propose that *H. miamia*'s brain is built from computationally pluripotent 'tiles', whose interactions generate coherent behavior. This architecture suggests that early brains arose by condensation of diffuse nerve nets into unregionalized brains, with regionalization evolving secondarily.

Introduction

The evolution of brains was a milestone in the history of animals: it likely enabled new behavior, including the first hunting lifestyles, and is thought to have triggered an evolutionary arms race between predators and prey that shaped the Cambrian explosion and modern animal diversity[1–3]. While modern animal brains vary substantially in their organization and complexity, they share some key features. Brains are centralized computing organs that serve as integrating centers; they collect sensory inputs and generate coherent organismal behavior[4,5]. Brains are highly regionalized, with specific regions specialized for specific tasks[6,7]. Brains are also stereotyped; within a species, all animals have the same brain organization. Brains likely evolved from ancient, diffuse nerve nets some 550-600 million years ago[8–10]. Indeed, the first animal nervous systems were likely diffuse nets, and extant cnidarians (and possibly ctenophores) retain a

version of diffuse nets[10,11]. Such nervous systems do not possess the core features of brains: they are not regionalized or stereotyped[12–14]. Instead, these features likely evolved during or after the origins of centralized brains.

Over the last two centuries, much has been learnt about the organization and function of diffuse nets. In the 1870s, Romanes and contemporaries, through a series of experiments involving incisions and amputations of jellyfish, first showed that cnidarians possess an unpolarized conducting substance distributed through their bodies[12,13,15]. A century later, electrophysiology and advances in histology reinforced these findings, and more recent work has begun to reveal detailed circuit mechanisms for how diffuse nets compute[16–20]. However, the large number of differences between diffuse nets and centralized brains has made it hard for biologists to imagine what the first brains may have looked like, or how nets transitioned to brains[10,21,22].

Acoel worms are ideally poised to shed light on these questions. Acoels belong to the likely sister lineage to all Bilateria[23–25]: i.e., all other animals with brains (Fig. 1a). Moreover, acoels are thought to possess some of the simplest brains; in other words, their nervous systems appear intermediate between diffuse nets and centralized brains[21,26–30]. However, acoel brains and behavior are poorly understood. Here, we study the acoel three-banded panther worm *Hofstenia miamia* (Fig. 1b). Using molecular labeling, amputation of brain regions, pose estimation, single-cell transcriptomics, and quantitative analysis of *H. miamia*'s brain and behavior, we find that *H. miamia* has a 'diffuse brain' unlike the brains of previously-studied bilaterians. We identify organizing principles for this diffuse brain, and suggest a trajectory for the evolution of the first brains.

The *H. miamia* brain lacks anatomical regionalization and stereotypy

In her taxonomic species description of *H. miamia,* Correa suggested that the brain was a subepidermal 'ganglionic ring' encircling the head[31]. Sixty years later, fluorescent *in situ* hybridization- and immunostaining-based studies revealed that the brain is a two-layered ring structure. The superficial layer contains reticulated neurite bundles wrapped around clusters of cell bodies, and the deeper layer contains densely-packed cells (*gad1+, pc2+*), separated from the superficial layer by an orthogonal grid of 'body wall' muscle[29]. Despite these advances in knowledge, the fine organization of the *H. miamia* brain remained unclear.

We used a variety of imaging techniques (live dyes, immunofluorescence, *in situ* hybridization, and electron microscopy) to visualize neural components at high resolution. Staining with a voltage dye labeled the entire superficial layer of the brain, showing that it is indeed a network of dense neuropil (i.e. a structure composed primarily of neural projections) (Fig. 1c,d; Fig. S1a-c). Tubulin and nuclear staining confirmed that each 'edge' of the network contains neurites running in parallel, that superficial cellular patches tile the neuropil, and that these often (but contrary to previous reports[29], not always) contain cells that coalesce into a sensory structure. We propose that this structure resembles a sensillum that is likely composed of a population of previously-described H1 receptors[32] (Fig. 1d; Fig. S1d). These cellular patches also contain muscle cell bodies (Fig. S1e).

Our results confirm that the *H. miamia* brain forms a subepidermal ring that encircles the head[33], with a dorso-ventral asymmetry: there are fewer network 'edges' in the neuropil near the ventral midline (Fig. S1a,b), possibly to accommodate the male copulatory apparatus[33]. Immunostaining with antibodies that label neurons, as well as electron microscopy, revealed that brain neurons are oriented orthogonal to the skin. Their cell bodies lie ~30-40μm beneath the skin, forming what were previously called 'layer 2 neurons'. This deeper layer is internal to the body wall muscle. The cell bodies that compose this layer project outward into the neuropil, ~10-20μm below the skin (Fig. 1e-h). In other words, the two 'layers' of the brain are primarily composed of the same interneurons, with deep cell bodies generating neurites that project peripherally and coalesce into dense, superficial neuropil (Fig. 1h). The neuropil lies immediately external to the body wall muscle (Fig. 1h)[29].

Immunostaining showed that neurons in the brain are sometimes multipolar, with 3-4 neurites emerging from the cell body and branching successively (Fig. 1e). Other neurons appear to be unipolar: e.g. Par3+ neurons (Fig. 1f). While the complete 3D structures of these neurons (and whether neurites are separable into distinct axons and dendrites) remains unclear, tubulin staining shows that they can have relatively long projections that extend well over 100μm (Fig. 1d; Fig. S1f). Sensory cells embedded in the skin project into the brain (Fig. 1e,g; Fig. S1g). Long cilia are visible near the mouth, likely due to the presence of distinct sensory cell type(s) (Fig. S1a-c,h). As previously reported, we detected three distinct innervated organs outside the brain. Tubulin staining showed that the frontal organ, putatively a sensory and secretory structure dorsal to the mouth[29], is innervated by long neural projections that fan out into the neuropil (Fig. S1i). The statocyst, putatively a gravity-sensing organ, lies in the anterior of the head, ventral to the brain but dorsal to the mouth[25,31] (Fig. S1j,k). We find that two neurons appear to innervate the statocyst laterally; this was previously referred to as the 'dorsal commissure'[29] (Fig. S1l). Immunostaining against Par3 reveals neurons that appear to innervate the penis[33] (Fig. S1m). The brain extends into a sparse posterior network that extends through the body (Fig. 1c). A similar network envelops the pharynx (Fig. S1n). In addition, labeling with a calcium dye revealed dense peripheral neural processes distributed through the skin (Fig. S1o; Video S1).

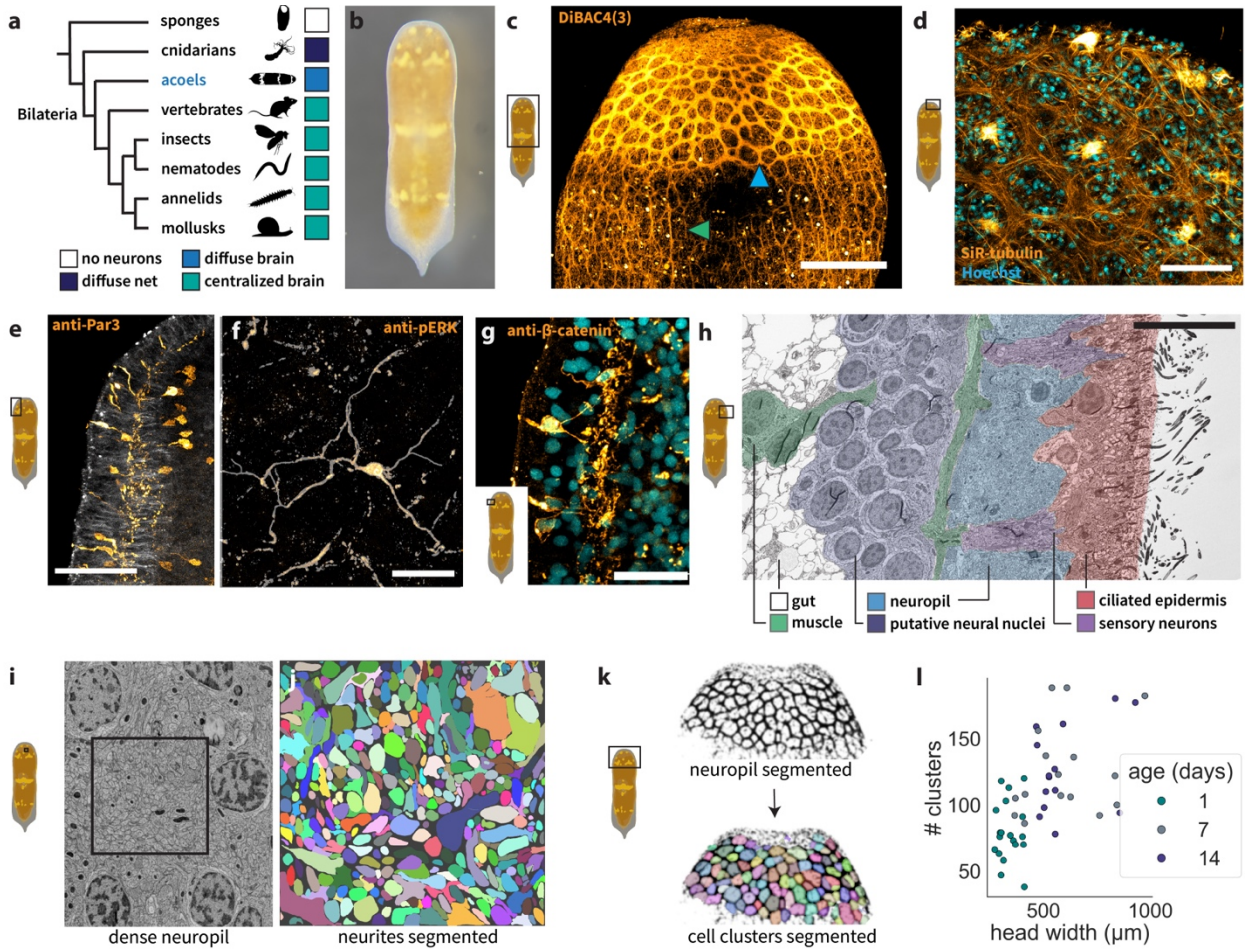

Figure 1: The organization of a diffuse brain. a) Simplified phylogeny of animals shows that acoel brains are likely intermediate between cnidarian diffuse nets and the centralized brains of typical bilaterians. b) Photograph of juvenile *Hofstenia miamia*. c) Staining with voltage dye reveals a superficial network of dense neuropil (blue arrow) that extends into a sparser posterior nerve net (green arrow). d) Close-up view of neuropil stained sparsely with tubulin dye (orange) reveals that the neuropil (orange) contains many neurites running in parallel, with cellular clusters (cyan) interspersed between neurite bundles. Sensory neurons (likely clusters of H1 cells; bright orange) are set within many of these patches. e) Cross-section of brain stained with a Par3 antibody reveals that the brain has two layers: superficial neuropil, and deeper cell bodies that project outward. f) Staining with an ERK antibody (z-projected segmentation overlaid) shows that brain interneurons can be multipolar, with a central cell body generating multiple neurites. g) Cross-section of brain stained with an antibody against β-catenin reveals another sensory neuron class (possibly H2[32]) with two projections that innervate brain neuropil. h) Electron microscopy cross-section shows the fine organization of the brain, confirming the relative configuration of tissue types within the head. The superficial neuropil (previously 'layer 1') is visible immediately beneath the skin, while neural cell bodies (previously 'layer 2') lie deeper in the tissue, internal to body wall muscle (green). Together, these layers compose the brain. i) Electron microscopy close-up of the brain shows dense neuropil; the box is a 6.7x6.7μm square. j) Segmenting neural projections within the highlighted box in (i) reveals over 400 neurites in a single section of neuropil. k) Segmentation of cellular clusters within neuropil allows quantification of brain structure and its variability. l) Quantifying the numbers of cellular clusters across brains reveals that, although cluster numbers

increase with age (i.e. days after hatching) and size (i.e. head width, a good proxy for overall body size[33]), worms vary widely in how many clusters they possess. Linear regression $p<0.0001$, $n=49$. Scale bars: 200μm (c), 50μm (d,e), 20μm (f,g), 10μm (h).

Next, to understand the internal structure of the neuropil, we used electron microscopy. We found that every region of neuropil contains hundreds of fine, reticulated neural projections (Fig. 1i,j). This density is suggestive of complex connectivity and the likelihood that this brain harbors a diversity of circuit motifs. Importantly, this organization is fundamentally different from cnidarian or ctenophore nerve nets, which are typically 2-3 neurites wide[17,34], rather than hundreds or thousands of neurites wide.

Together, these results describe the structure of the *H. miamia* brain. Most remarkably, we find that this brain is almost entirely devoid of internal anatomical regionalization: within the neuropil, we detect no distinct regions, lobes, or stereotyped commissures. Regionalization is a core feature of typical bilaterian brains: across phyla as diverse as mollusks, arthropods, nematodes, vertebrates, and annelids, different brain regions have different structures and functions, and these regions are in the same relative positions across individuals within a species (and often over hundreds of millions of years)[6,35–37]. Given its lack of regionalization, the *H. miamia* brain is fundamentally different. Next, we asked whether this brain displayed any stereotypy in its structure.

To test for stereotypy, we quantified brain structure by segmenting and counting the sensory patches that tile the neuropil (Fig. 1c,d,k). We found that as worms grow during juvenile development, the number of these patches increases (Fig. 1l). However, even among worms of the same age, size, and rearing environment, we found an order of magnitude of variation in the number of patches within their brains (Fig. 1k,l). Thus, while every brain has similar network topology, every brain is also different in its exact shape. This would imply that the same neural circuits cannot be in the same relative locations across worms. In other words, the *H. miamia* brain, unlike previously-studied bilaterian brains, appears to lack regionalization and stereotypy, and it suggests that this brain must be organized differently.

***H. miamia* brain regions are computationally pluripotent**

The lack of anatomical regionalization within the *H. miamia* brain suggests that function may not be regionalized either. Taking advantage of *H. miamia*'s ability to survive and regenerate the brain and its function after major wounding, we sought to assess functional brain regionalization by amputating brain regions and studying their subsequent behavior.

To study the consequences of removing brain regions, we first developed an ethologically-relevant behavioral assay. *H. miamia* are thought to forage by hunting other small marine invertebrates in the wild, and they eat brine shrimp or rotifers in the lab. We developed a foraging assay in which worms were presented a choice between a block of agarose with prey rotifers embedded in it and a control block of agarose with no prey. We found that hungry worms navigated to the agarose with rotifers and attempted attacks (Video S2), while continuously fed (Fig. 2a-c) worms did not. Next, to ask whether this foraging behavior ceased

175 when the worms had consumed enough food: i.e., to ask whether hunger in *H. miamia* had the
176 same motivational properties as in typical bilaterians[38], we first starved worms and then fed
177 them for 6h prior to studying foraging. These sated worms did not forage, confirming that hunger
178 and satiety are opposing motivational forces that regulate foraging behavior (Fig. S2a). These
179 data demonstrate the validity of this foraging assay, and show that worms continuously assess
180 their internal states, integrate this with sensory input, and select appropriate actions to forage.
181 Next, we asked how foraging behavior was affected by amputating brain regions. First,
182 we performed a transverse amputation to separate heads from tails in starved worms. We found
183 that tail fragments, which lack brains, did not forage and indeed were unable to move (Fig. S2b),
184 while head fragments foraged normally both immediately after amputation and two days later
185 (Fig. 2d), when their wounds have closed but new tails have not yet formed[25,39]. This shows that
186 the posterior nerve net cannot independently generate coherent movement or induce goal-
187 directed behavior, and that the brain is necessary for coordinated behavior. We then removed
188 the right half of the head (Fig. S2c). Worms missing half their heads did not display obvious
189 movement defects (Fig. S2d). More importantly, we found that two days after amputation,
190 worms missing half their heads foraged similarly to intact worms, when the wound had closed
191 but new tissue had not yet emerged (Fig. 2e; Fig. 2Si,j). Similarly, removing the dorsal half of
192 the head did not affect foraging (Fig. 2e). This robustness to amputation is not the result of rapid
193 regeneration; quantifying brain structure showed that three days after amputation, brains had
194 not yet regenerated missing tissue (Fig. S2i,j). Removing the mouth resulted in a reduction in
195 foraging behavior (Fig. 2e; Fig. S2h,n), although we detected no obvious movement defect (Fig.
196 S2d).
197 To study the capture phase of foraging, we next provided worms access to a controlled
198 density of free-moving rotifers for a defined time period, and quantified the number of rotifers
199 they consumed. Worms missing half their heads consumed similar numbers of rotifers to intact
200 starved controls. Worms missing their mouths consumed fewer rotifers than intact worms or
201 those missing half their heads, but significantly more than intact fed worms did (Fig. 2f).
202 Together, these data suggest that amputation of the mouth may result in a chemosensory-
203 specific defect, consistent with the presence of specific sensory cell types near the mouth (Fig.
204 S1a-c,e)[32]. These data also show that amputation of large fractions of the brain, including half
205 the mouth (i.e. when removing the right or dorsal half of the head) do not prevent worms from
206 executing all tasks necessary for foraging behavior. In addition, these amputations include
207 conditions in which the statocyst, frontal organ and associated neurons were damaged or
208 entirely removed, showing that these organs are dispensable for all aspects of foraging
209 behavior.
210 Next, we removed wedges of differing size from the heads of worms: a small wedge, two
211 bilateral wedges (to account for the possibility of bilaterally-symmetric, redundant regions with
212 specialized roles), and a large wedge that removed the majority of the head (Fig. S2k; Video
213 S3). We found that worms foraged robustly despite the loss of these arbitrary brain regions (Fig.
214 2g). In many of these conditions, wound closure involves the attachment of dorsal and ventral
215 wound edges[39], likely connecting brain regions that are normally separate (Fig. S2g). Despite

these abnormal structural configurations, worms displayed robust foraging behavior. To further control for the possibility of rapid regeneration, or lateralized function, we also amputated the left half of the head and studied foraging behavior both immediately after amputation and two days later (Fig. S2l,m). Again, we found that foraging behavior is robust to these amputations. Finally, we conducted a wide variety of additional amputations, removing wedges of varying size and location from worm heads. These also did not affect foraging behavior (Fig. S2n).

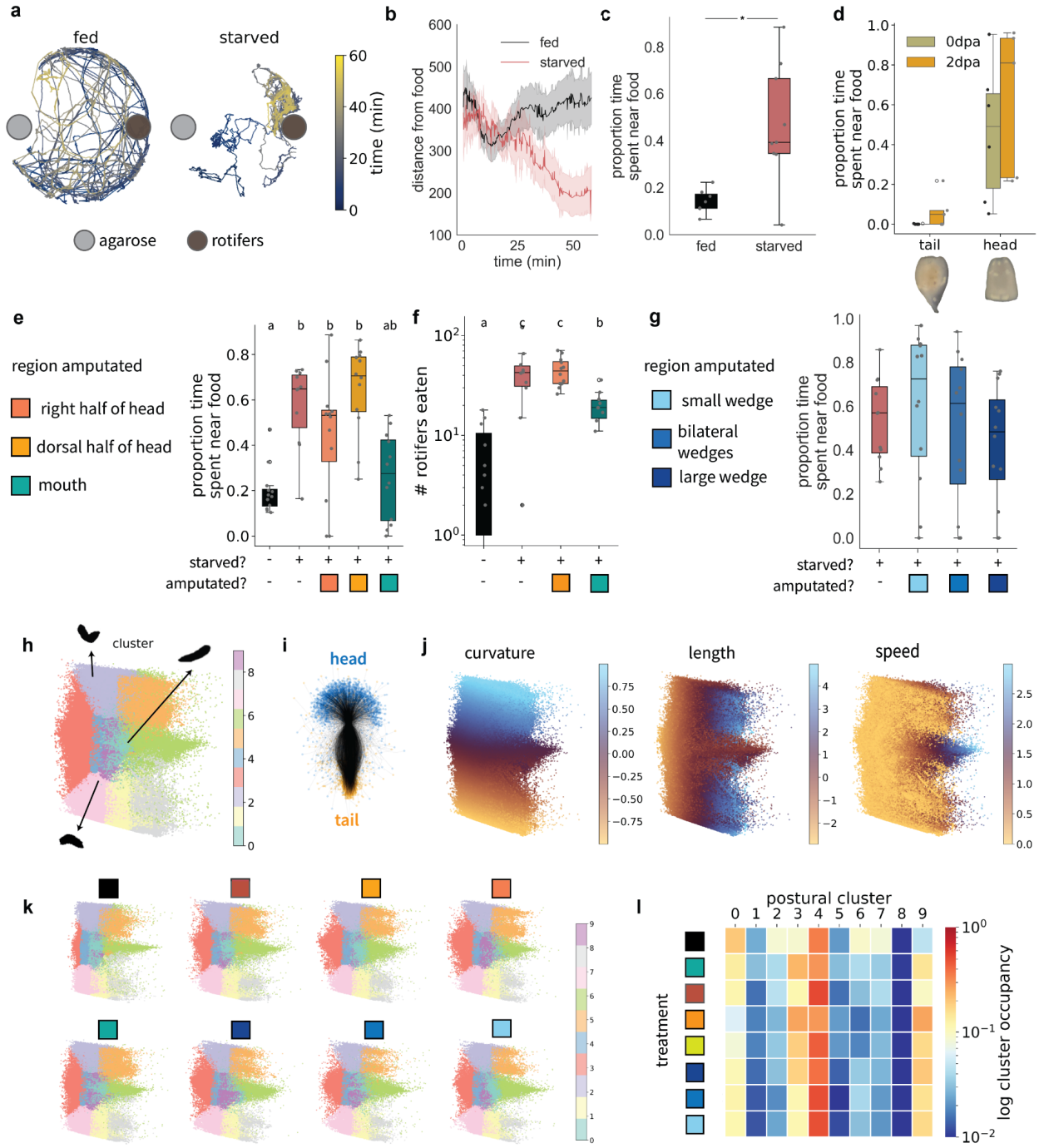

Figure 2: *H. miamia*'s foraging behavior is robust to brain amputations. a) Examples of tracks for a representative fed and starved worm presented a choice between agarose blocks with and without rotifers. Trajectories colored by time. b) Starved worms approach the rotifers; fed worms generally do not (see also Fig. S2l). Error band represents standard error. c) Quantifying this behavior as the proportion of time spent near food provides a robust metric of foraging behavior (see Methods); t-test FDR-corrected $p=0.03, n>=6$, data also used in Fig. S2l. d) Amputated tails do not forage, either immediately (0 dpa: t-test $p=0.01$, $n>=5$) or two days after (2dpa: t-test $p=0.01$, $n>=5$) amputation, while amputated heads do. e) Amputation of the right or dorsal half of the head does not affect foraging behavior, while amputation of the mouth inhibits foraging. f) Quantifying the number of rotifers in the guts of worms shows that amputation of half the head does not affect feeding. Letters above boxplots in (e) and (f) indicate significance levels after one-way ANOVA and Tukey post-hoc tests; corrected $ps<0.05$. g) Removing tissue of varied size and geometry from the brain also does not affect foraging behavior. One-way ANOVA $p=0.54$, $n>=10$. h) A low-dimensional postural space (i.e. of the first two principal components of the space defined by curvature, length, and speed) captures major elements of *H. miamia*'s postures during foraging, with k-means cluster identities shown, and representative worm postures overlaid for some clusters. See Table S1 for mean values of curvature, length, and speed for each cluster. i) Overlaid and aligned splines fitted to tracked worm midlines from a representative worm show the space of possible postures - and especially curvature - for a worm. j) Normalized curvature, worm length (z-scored within worm), and speed appear as gradients within the postural space. k) Projecting amputated worm postures into this postural space shows that irrespective of amputation, all worms express all elemental postures. l) Comparing postural cluster occupancies shows that fed, intact worms are most different in their postural behavior, while amputated worms generally display only minor differences in occupancy compared to starved, intact worms. See Tables S2 and S3 for statistics.

These data show that worms can forage successfully even after the removal of large, arbitrary majorities of brain tissue. Nonetheless, it is possible that worms with amputated brain regions experience some subtle behavioral defects. We reasoned that these hypothetical defects would likely be in their motor coordination, since the worms were clearly able to perform chemosensation, internal state sensing, and select actions necessary for foraging. We therefore quantified worm posture during foraging at high resolution, by tracking keypoints on the worm's midline. Preliminary observations of the worms suggested that their postural dynamics are well represented by three features: the speed they travel at, the curvature of their midlines, and their body lengths. Using these data, we generated a low-dimensional postural space during foraging from starved worms with intact brains (Fig. 2h-j). The boundaries of the occupied region of this space (Fig. S3a) reveal core biomechanical constraints on *H. miamia*'s movement. *H. miamia* has two motor systems: epidermal cilia (see Fig. 1h) polarized along the anterior-posterior axis that beat to produce thrust and allow forward gliding, and distributed sets of muscle (including orthogonal grid of body wall muscle) that contort to allow turning. Worms in sharp turns experience no forward displacement, likely because the cilia in different body regions are beating in different directions. Worms are fastest when at intermediate length, but stretch and compress themselves frequently (Fig. S3a).

Next, we used k-means clustering to segment elemental postural states within this space (Fig. 2h; Table S1), and then projected onto this space similar data from fed worms with intact

brains as well as starved worms subjected to numerous amputations (i.e. data from Fig. 2f,g). We found that fed, intact worms were most different in their postural expression, consistent with their lack of foraging behavior (Fig. 2k,l; Fig. S3b,c; Table S2,3). We found that arbitrary amputations of brain regions do not affect the generation of postures or the transitions between postures, although we detected some subtle effects on relative occupancy of specific postural states and transitions (Fig. S3b,c; Table S2,3). In addition, we did not detect differences in turning bias after amputations of the right half the brain (Fig. 2k,l; Video S3), showing that brain regions locally generate postural states necessary for both left and right turns, rather than implementing lateralized control as in many other Bilateria[40,41]. In other words, these data suggest that most or all motor commands can be generated in any or all brain regions, control motor behavior locally, and can be transmitted body-wide.

Together, these data show that the *H. miamia* brain exhibits little functional regionalization. Instead, most or all brain regions are computationally 'pluripotent': i.e., most or all neural computations necessary for foraging occur in many or all regions of the brain, likely simultaneously. These computations include sensory processing and integration, internal state assessment, selecting actions, and motor control of most or all muscular and ciliary motor systems - i.e. the generation of all static postures and their sequences.

Neural cell types lack regionalization within the brain, consistent with a tiled organization

How might such a brain be organized? We hypothesized that the brain is composed of tessellating tiles of similar neural circuits, each of which is computationally 'pluripotent'. If this were true, we would expect these tiles to be composed of ensembles of similar neural cell types. Conversely, detecting substantial regionalization in the locations of individual cell types would disprove this hypothesis. Previous work in *H. miamia* found that neural markers are distributed across the entire brain[42,43]. However, many of these markers are expressed in large subsets of neural cell types, and we reasoned that, as in typical brains[44,45], markers of sparse cell types could exhibit greater regionalization. To test the tiling hypothesis more directly, we therefore sought markers of sparse cell types. We first integrated all relevant *H. miamia* single-cell RNA sequencing datasets[42,46] (Fig. S4a), selected all neurons (Fig. S4b,c), and reclustered them to identify individual neural cell types (Fig. S4d,e). Analyzing this dataset of 15,262 cells, we identified 25 putative neural clusters with specific markers for most clusters (Fig. 3a). We selected markers likely to have functional relevance from this list. To overcome the possibility that some neural markers may not be represented in this dataset due to technical limitations, we also included evolutionarily conserved genes with likely roles in neurotransmitter synthesis or processing pathways that were previously identified[47–49].

We used fluorescence *in situ* hybridization to assess the distribution of neurons expressing these genes in worms. Of 42 genes that we screened (Table S4), we identified 24 with neural expression, including several that sparsely labeled neurons within the head and others that labeled large subsets of neurons (Fig. 3b; Fig. S5). Qualitatively, all identified cell populations appeared largely or entirely distributed across the brain (Fig. S5). To systematically test regionalization, we quantified gene expression patterns for all markers in the head

(including previously published markers for all qualitative neural expression classes, but excluding markers of sensory neuron populations in the mouth and elsewhere in the body), and we computed two density-corrected indices of regionalization for each gene (Fig. 3c, see Methods). As expected, markers expressed in large subsets of neural types did not display regionalization (Fig. 3d). Moreover, irrespective of the sparseness of gene expression, markers had minimal regionalization on both indices (Fig. 3d). These data are consistent with the tiling hypothesis. Taken together, our anatomical, behavioral and molecular data all find little evidence that the *H. miamia* brain contains specialized regions, and instead may be composed of repeating, computationally pluripotent units - which we term ‘circuit tiles’.

How might a circuit tile be organized? A few possibilities present themselves. First, it is possible that the patches of sensory cells that tile the brain, with surrounding neuropil, represent computationally pluripotent circuit tiles: this would lead to a brain containing hundreds of tiles across its surface in a juvenile worm. Alternatively, it is possible that each tile contains all neuron types, in which case its size would be set by the distance between neighboring cells of the sparsest type - i.e., tens of tiles in a juvenile worm brain. It is also possible that tiles vary in their exact composition and architecture. We do not wish to imply that tiles necessarily have higher within-unit than between-unit connectivity; our anatomical studies of the brain (e.g. Fig. 1d) suggest that there is likely extensive lateral connectivity across all visible regions of the neuropil. Regardless, the worm’s anatomy ensures that every tile contains connections to the motor systems: epidermal cilia, peripheral, body wall, parenchymal and pharyngeal muscle. In addition, tiles likely contain one and possibly multiple sensory cells or organs, which allows each tile to locally receive some sensory input and to transmit most or all motor commands.

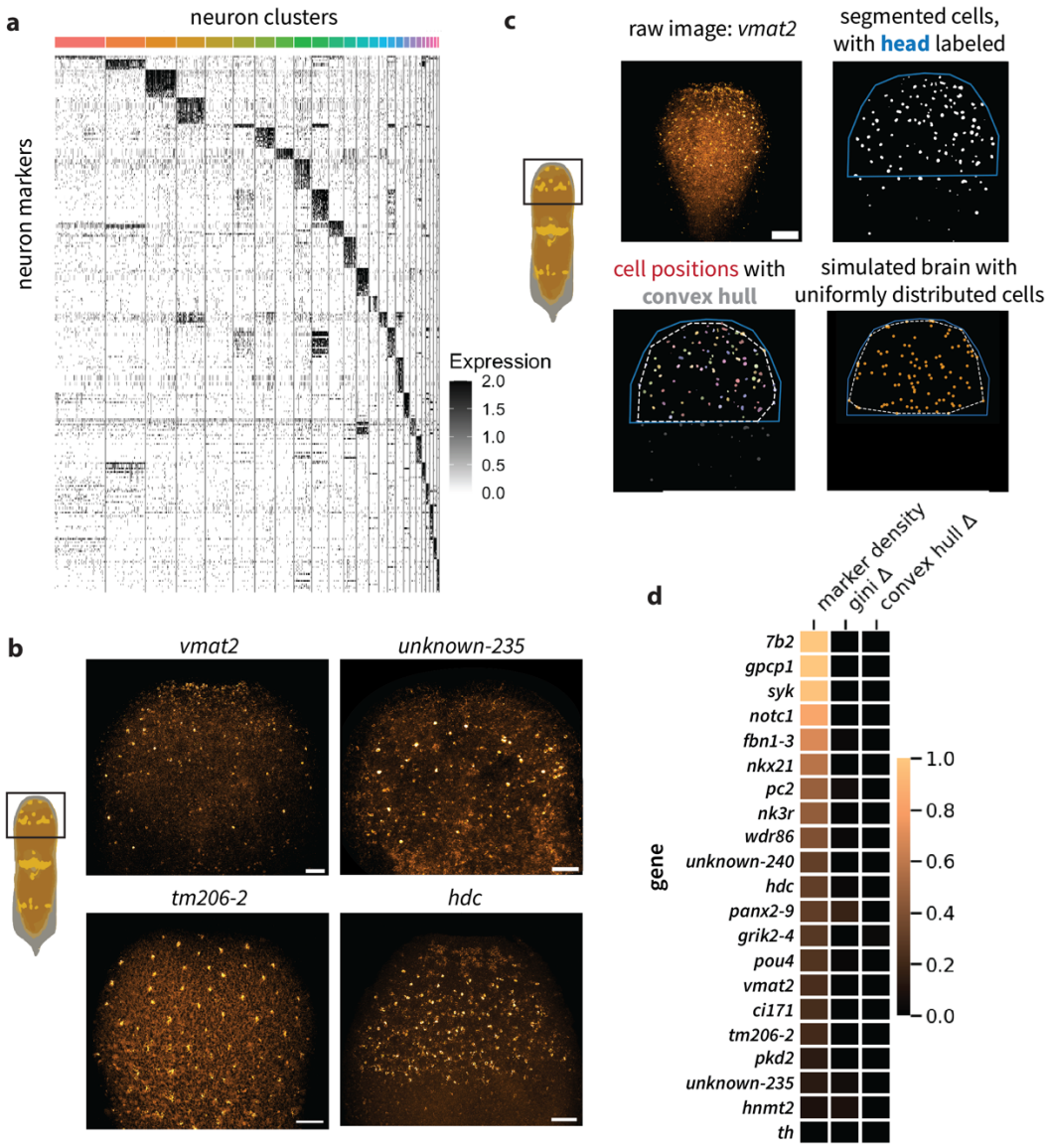

Figure 3: Neural cell types are distributed across the *H. miamia* brain. a) Heatmap of top 20 markers from each neural cluster shows that many markers are expressed in specific clusters, suggesting that these are cell-type specific markers. b) Fluorescence in situ hybridization of neural markers reveals that several label sparse, distributed populations. c) Outline of analysis of spatial distributions of markers: pixel classification to segment fluorescent puncta (corresponding to cell bodies for sparse markers), fitting convex hull to segmented cells and calculating the ratio of its area to the area of the polygon describing the brain, and simulating brains with uniformly distributed cells with the same density as the empirical data. d) Neural markers exhibit little regionalization across a wide range of cell densities, as assessed by two metrics: the difference in gini coefficients for brain regions containing expression between real brains and simulated uniform brains (gini Δ), and the difference in the proportion of brain area containing cells between real brains and simulated uniform brains (convex hull Δ). Scale bars: 100μm (c), 50μm (b).

On how a diffuse brain computes

The unusual organization of the *H. miamia* brain raises several questions. For instance, why does it contain multiple circuit tiles, when fewer, or perhaps one, should do? First, we reanalyzed our experiment in which we amputated different amounts of brain tissue (Fig. 2g). Analyzing these data as a function of approximately how much brain tissue was removed (rather than as a set of discrete perturbations), we found that although no amputation treatment prevented worms from foraging successfully, worms missing more brain tissue took slightly longer to find immobilized rotifers (Fig. 4a; Fig. S6a). This was not because the worms were mechanically impaired or took longer to travel the same distance (Fig. S6b); instead, worms missing more brain tissue may be worse at locating prey. To test whether this effect was reproducible, we diluted the prey stimulus by reducing the concentration of immobilized rotifers presented to the worms. Worms missing ~80% of their brains foraged successfully when presented with high concentrations of immobilized rotifers, but were unable to detect rotifers at a low concentration (Fig. 4b), suggesting that more brain tiles may allow greater perceptual resolution and therefore behavior resulting in higher fitness. These results also showed that presenting the worms with challenging tasks can reveal subtle effects of amputation. To conclusively test the idea that more tiles allow better estimation of prey position, and to identify any other subtle effects of amputation, we sought to challenge the worms further, in a more controlled and ethologically-relevant way.

We studied the hunting behavior of worms pursuing a single free-moving prey (i.e. a brine shrimp) - a challenging task in which nearly all hunts end in failure to consume the prey within the duration of the assay (we recorded 1/12 successful captures among intact worms). We jointly tracked the positions of the worm and the shrimp (Fig. 4c; Video S4). Shrimp had lower velocity autocorrelations when in the presence of a worm (Fig. S6c), showing that they actively evade being hunted. Similarly, worms displayed lower velocity autocorrelations when the shrimp was present (Fig. S6d), showing that they actively hunt escaping prey. Worms with half their heads amputated displayed similar dynamics, but had slightly lower velocity autocorrelations compared to intact worms, specifically during foraging (Fig. S6d). These data suggest that amputation has a subtle impact on how worms hunt, but has little impact on the worms' ability to detect stimuli or execute movements. We therefore asked whether amputated worms are worse at hunting.

We found that worms were able to track shrimp, moving towards the trajectory of the shrimp, with the worm lagging the shrimp by 20-30 seconds (Fig. 4c,d). Worms missing half their heads were poorer at tracking shrimp (Fig. S6e). Next, we removed increasing fractions of brain tissue from another cohort of worms. Analysis of postural dynamics in this richer behavioral setting confirmed our previous finding that all postures and postural sequences are robust to large-scale amputation, and can be generated by arbitrary brain regions (Fig. S6f-j). Indeed, relative occupancy of postural states, and transitions between postures, were also largely indistinguishable between intact and amputated worms (Fig. S6i,j; Table S5,S6). However, we found that worms missing greater fractions of brain tissue displayed poorer

tracking (Fig. 4d,e). This reinforces the notion that more brain tiles allow greater perceptual resolution.

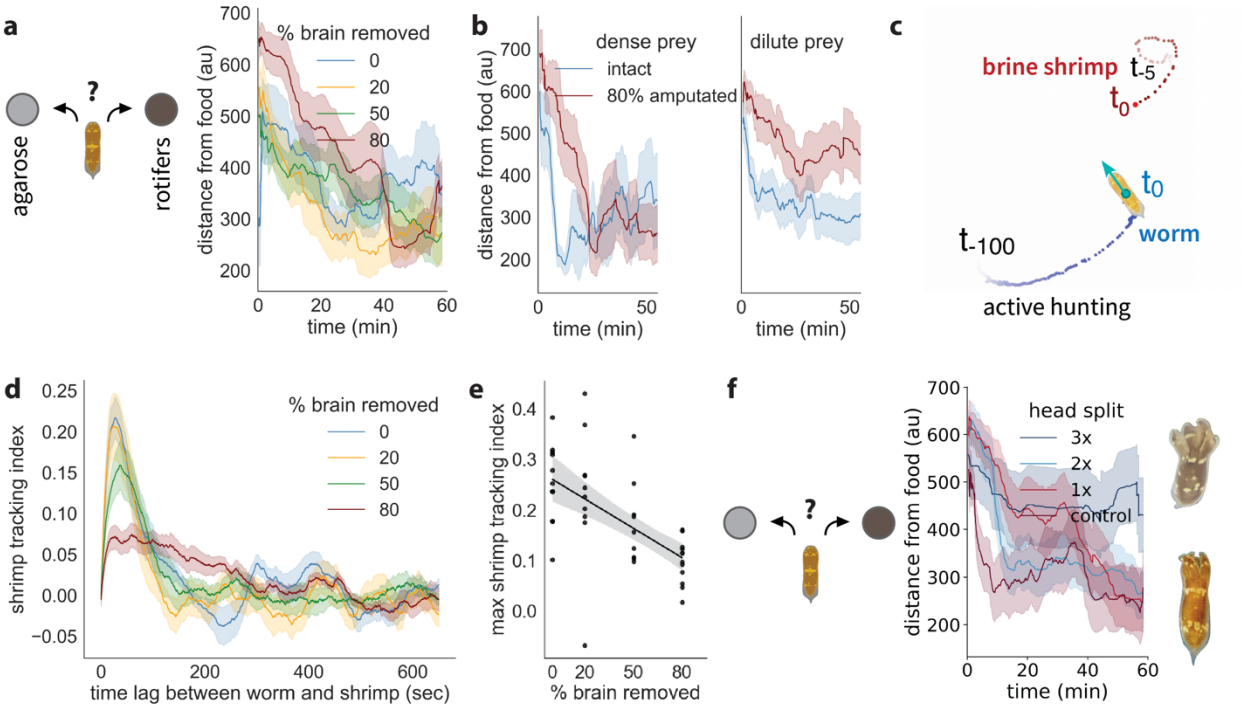

Figure 4: The collective behavior of circuit tiles. a) Worms missing greater fractions of their brain take longer to locate rotifers embedded in agarose (schematic shows assay design: worms choose between agarose containing rotifers and plain agarose, as in Fig. 2). b) Reproducing this effect, worms with ~80% of their brain missing are unable to detect a low density of rotifers embedded in agarose, and are slower to detect rotifers at high density. High-density prey, intact vs amputated t-test for proportion of time spent near food: p=0.8, n=5 per treatment. Low-density prey, intact vs amputated t-test for proportion of time spent near food: p=0.02,n>=14 per treatment. c) Schematic of hunting behavior assay, showing joint tracking of worm and its prey shrimp. The recent trajectory of the shrimp is shown in red (5s); the recent trajectory of the worm is shown in blue (100s). The cyan arrow shows the direction of motion of the worm. d) Worms track shrimp positions; worms missing more brain display poorer tracking (e). Linear regression p<0.0001, n=38. f) Splitting the brain into six fragments inhibits foraging behavior one hour after incision, with worms unable to detect rotifers embedded in agarose. Tukey post-hoc tests for mean distance from food in the final third of the assay, 3x vs other treatments p<=0.02, n>=9 per treatment. All error bands represent standard error.

Finally, we asked how brain tiles collectively generate coherent organismal behavior. One possibility is that brain tiles compute independently, with the motor systems effectively summing their separate outputs: i.e., the *H. miamia* brain would perform degenerate computations. Alternatively, it is possible that tiles interact, allowing computations to emerge from their collective activity: distributed computation. To test this hypothesis, we split heads into increasing numbers of fragments. Each fragment remained attached to the body; i.e. the number of brain tiles stays constant. We reasoned that this would disrupt interactions between

brain tiles, but allow them to generate motor outputs independently. Consistent with this hypothesis, worms with their heads split into two or four fragments foraged similarly to intact worms, but worms with their heads split into six fragments did not (Fig. 4f). These worms were capable of coordinated movement, indicating that this defect was not mechanical (Video S5). Together with our anatomical data showing extensive lateral connectivity (Fig. 1d; Fig. S1d), this suggests that circuit tiles do indeed interact.

There are two extreme modes of interaction that might be useful to consider in the context of decision-making. The first is one where noise or errors decrease simply by virtue of having more identical copies, a physical realization of the law of large numbers. The second is one where a nonlinear interaction between the tiles leads to a phase transition or bifurcation as the number of tiles crosses a threshold. We are currently unable to distinguish between these possibilities. Regardless, these results suggest that at least some computations in the *H. miamia* brain are distributed, with coherent organismal behavior emerging from the collective activity of interacting brain tiles.

Conclusion

Nearly a century ago, Lashley lesioned cortical regions from the brains of rats, and found that they could still perform spatial navigation and solve mazes[50,51]. From these and earlier experiments, he devised principles for brain organization: the principle of equipotentiality (effectively: brain regions are computationally pluripotent - or equipotent) and the principle of mass action (effectively: more brain is better). Further work showed that these principles do not accurately describe the organization of the mammalian brain, although the nature and extent of regionalization within cortex continues to be debated[7,52–54]. Strikingly, our results show that *H. miamia*'s diffuse brain, unlike typical bilaterian brains, does indeed obey Lashley's principles. We find that the *H. miamia* brain is not regionalized anatomically, cellularly, or functionally, and that all brain regions appear capable of performing most or all neural computations. We propose that the brain is composed of tessellating tiles of pluripotent neural circuits, and that these tiles interact to implement distributed computations. More generally, our results suggest that the space of realized brain forms may be broader than was previously assumed; brains do not have to be highly regionalized or stereotyped.

How the first brains were organized remains unknown, but our new understanding of the brain of an acoel lends support to a concrete trajectory of brain evolution. In this view, diffuse nerve nets were first concentrated in early animal heads (as, or after, they first evolved bilateral symmetry), retaining the ancestral lack of regionalization and stereotypy that typifies current diffuse nets. Perhaps these nascent brains then evolved elaborations for dense connectivity, new molecular signaling systems[47], and possible new neural morphology and circuit motifs[35,55] - coalescing in new behavioral affordances. Regionalized, stereotyped circuits likely evolved later, bringing forth the ground plan that enabled expansions into a diversity of bilaterian brains and a corresponding range of complex behavioral repertoires.

454 **References**

455 1. Bicknell, R. D. C., Campione, N. E., Brock, G. A. & Paterson, J. R. Adaptive responses in
456 Cambrian predator and prey highlight the arms race during the rise of animals. *Curr. Biol.*
457 **35**, 882–888.e2 (2025).
458 2. Monk, T. & Paulin, M. G. Predation and the origin of neurones. *Brain Behav. Evol.* **84**, 246–
459 261 (2014).
460 3. Vinn, O. Traces of predation in the Cambrian. *Hist. Biol.* **30**, 1043–1049 (2018).
461 4. Pagán, O. R. The brain: a concept in flux. *Philos. Trans. R. Soc. Lond. B Biol. Sci.* **374**,
462 20180383 (2019).
463 5. Richter, S. *et al.* Invertebrate neurophylogeny: suggested terms and definitions for a
464 neuroanatomical glossary. *Front. Zool.* **7**, 29 (2010).
465 6. Kandel, E. R., Schwartz, J. H., Jessell, T. M., Siegelbaum, S. A. & Hudspeth, A. J.
466 *Principles of Neural Science, Fifth Edition (Principles of Neural Science (Kandel))*. 1760
467 (McGraw-Hill Medical, 2012).
468 7. Szczepanski, S. M. & Knight, R. T. Insights into human behavior from lesions to the
469 prefrontal cortex. *Neuron* **83**, 1002–1018 (2014).
470 8. Carlisle, E., Yin, Z., Pisani, D. & Donoghue, P. C. J. Ediacaran origin and Ediacaran-
471 Cambrian diversification of Metazoa. *Sci. Adv.* **10**, eadp7161 (2024).
472 9. Budd, G. E. & Mann, R. P. Two notorious nodes: A critical examination of relaxed molecular
473 clock age estimates of the bilaterian animals and placental mammals. *Syst. Biol.* **73**, 223–
474 234 (2024).
475 10. Arendt, D., Tosches, M. A. & Marlow, H. From nerve net to nerve ring, nerve cord and
476 brain--evolution of the nervous system. *Nat. Rev. Neurosci.* **17**, 61–72 (2016).
477 11. Arendt, D. Elementary nervous systems. *Philos. Trans. R. Soc. Lond. B Biol. Sci.* **376**,
478 20200347 (2021).
479 12. Romanes, G. J. XI. The Croonian lecture.--Preliminary observations on the locomotor

system of medusæ. *Philos. Trans. R. Soc. Lond.* **166**, 269–313 (1876).

13. Anctil, M. *Dawn of the Neuron*. (McGill-Queen's University Press, Montréal, QC, Canada, 2015).
14. Courtney, A. *et al.* Characterization of geometric variance in the epithelial nerve net of the ctenophore Pleurobrachia pileus. *J. Comp. Neurol.* **530**, 1438–1458 (2022).
15. Mackie, G. O. The first description of nerves in a cnidarian: Louis Agassiz's account of 1850. in *Coelenterate Biology 2003* 27–32 (Springer Netherlands, Dordrecht, 2007).
16. Weissbourd, B. *et al.* A genetically tractable jellyfish model for systems and evolutionary neuroscience. *Cell* **184**, 5854–5868.e20 (2021).
17. Dupre, C. & Yuste, R. Non-overlapping Neural Networks in Hydra vulgaris. *Curr. Biol.* **27**, 1085–1097 (2017).
18. Jékely, G. & Yuste, R. Nonsynaptic encoding of behavior by neuropeptides. *Curr. Opin. Behav. Sci.* **60**, 101456 (2024).
19. Anderson, P. A. & Spencer, A. N. The importance of cnidarian synapses for neurobiology. *J. Neurobiol.* **20**, 435–457 (1989).
20. Satterlie, R. A. Cnidarian Nerve Nets and Neuromuscular Efficiency. *Integr. Comp. Biol.* **55**, 1050–1057 (2015).
21. Martinez, P. & Sprecher, S. G. Of Circuits and Brains: The Origin and Diversification of Neural Architectures. *Frontiers in Ecology and Evolution* **8**, (2020).
22. Holland, N. D. Early central nervous system evolution: an era of skin brains? *Nat. Rev. Neurosci.* **4**, 617–627 (2003).
23. Álvarez-Presas, M., Ruiz-Trillo, I. & Paps, J. Novel genomic approaches support Xenacoelomorpha as sister to all Bilateria. *Research Square* (2024) doi:10.21203/rs.3.rs-5529390/v1.
24. Cannon, J. T. *et al.* Xenacoelomorpha is the sister group to Nephrozoa. *Nature* **530**, 89–93 (2016).

506 25. Srivastava, M., Mazza-Curll, K. L., van Wolfswinkel, J. C. & Reddien, P. W. Whole-Body
507 Acoel Regeneration Is Controlled by Wnt and Bmp-Admp Signaling. *Curr. Biol.* **24**, 1107–
508 1113 (2014).
509 26. Reuter, M. *et al.* Organisation of the nervous system in the Acoela: an immunocytochemical
510 study. *Tissue Cell* **33**, 119–128 (2001).
511 27. Hejnol, A. & Martindale, M. Q. Acoel development supports a simple planula-like
512 urbilaterian. *Philos. Trans. R. Soc. Lond. B Biol. Sci.* **363**, 1493–1501 (2008).
513 28. Bourlat, S. J. & Hejnol, A. Acoels. *Curr. Biol.* **19**, R279–280 (2009).
514 29. Hulett, R. E., Potter, D. & Srivastava, M. Neural architecture and regeneration in the acoel
515 Hofstenia miamia. *Proc. Biol. Sci.* **287**, 20201198 (2020).
516 30. Achatz, J. G. & Martinez, P. The nervous system of Isodiametra pulchra (Acoela) with a
517 discussion on the neuroanatomy of the Xenacoelomorpha and its evolutionary implications.
518 *Front. Zool.* **9**, 27 (2012).
519 31. Corrêa, D. D. Two New Marine Turbellaria from Florida. *Bull. Mar. Sci.* **10**, 208–216 (1960).
520 32. Todt, C. & Tyler, S. Ciliary receptors associated with the mouth and pharynx of Acoela
521 (Acoelomorpha): a comparative ultrastructural study: Ciliary receptors of Acoela. *Acta Zool.*
522 **88**, 41–58 (2006).
523 33. Chandra, V., Tseng, S. E., Kann, A. P., Marcela Bolanos, D. & Srivastava, M.
524 Developmental, regenerative, and behavioral dynamics in acoel reproduction. *Elife*
525 RP105712 (2025).
526 34. Keramidioti, A. *et al.* A new look at the architecture and dynamics of the Hydra nerve net.
527 *Elife* **12**, (2024).
528 35. Bullock, T. H. & Horridge, G. A. *Structure and Function in the Nervous Systems of*
529 *Invertebrates*. (W.H. Freeman, New York, NY, 1965).
530 36. Scheffer, L. K. *et al.* A connectome and analysis of the adult Drosophila central brain. *Elife*
531 **9**, e57443 (2020).

532 37. Montague, T. G. *et al.* A brain atlas for the camouflaging dwarf cuttlefish, Sepia bandensis.
533 *Curr. Biol.* **33**, 2794–2801.e3 (2023).
534 38. Anderson, D. J. & Adolphs, R. A framework for studying emotions across species. *Cell* **157**,
535 187–200 (2014).
536 39. Kann, A. P. & Srivastava, M. Cooperation between proximate cell layers drives large-scale
537 wound closure prior to whole-body regeneration. *bioRxiv* 2025.02.03.636261 (2025).
538 40. Büschges, A., Scholz, H. & El Manira, A. New moves in motor control. *Curr. Biol.* **21**, R513–
539 24 (2011).
540 41. Büschges, A. & Ache, J. M. Motor control on the move: from insights in insects to general
541 mechanisms. *Physiol. Rev.* **105**, 975–1031 (2025).
542 42. Hulett, R. E. *et al.* Acoel single-cell atlas reveals expression dynamics and heterogeneity of
543 adult pluripotent stem cells. *Nat. Commun.* **14**, 2612 (2023).
544 43. Hulett, R. E., Rivera-López, C., Gehrke, A. R., Gompers, A. & Srivastava, M. A wound-
545 induced differentiation trajectory for neurons. *Proc. Natl. Acad. Sci. U. S. A.* **121**,
546 e2322864121 (2024).
547 44. Court, R. *et al.* Virtual Fly Brain-An interactive atlas of the Drosophila nervous system.
548 *Front. Physiol.* **14**, 1076533 (2023).
549 45. Shainer, I. *et al.* A single-cell resolution gene expression atlas of the larval zebrafish brain.
550 *Sci. Adv.* **9**, eade9909 (2023).
551 46. Rock, A. Q. & Srivastava, M. Totipotency and high plasticity in an embryo with a
552 stereotyped, invariant cleavage program. *bioRxiv* 2025.02.12.637942 (2025).
553 47. Goulty, M., Botton-Amiot, G., Rosato, E., Sprecher, S. G. & Feuda, R. The monoaminergic
554 system is a bilaterian innovation. *Nat. Commun.* **14**, 3284 (2023).
555 48. Thiel, D., Franz-Wachtel, M., Aguilera, F. & Hejnol, A. Xenacoelomorph neuropeptidomes
556 reveal a major expansion of neuropeptide systems during early bilaterian evolution. *Mol.*
557 *Biol. Evol.* **35**, 2528–2543 (2018).

558 49. Hsiao, J., Deng, L. C., Chalasani, S. & Edsinger, E. Numerous expansions in TRP ion
559 channel diversity highlight widespread evolution of molecular sensors in animal
560 diversification. *bioRxiv* 2021.11.14.466824 (2021).
561 50. Lashley, K. S. *Brain Mechanisms and Intelligence: A Quantitative Study of Injuries to the*
562 *Brain*. vol. 186 (University of Chicago Press, Chicago, 1929).
563 51. Nadel, L. & Maurer, A. P. Recalling Lashley and reconsolidating Hebb. *Hippocampus* **30**,
564 776–793 (2020).
565 52. Petersen, S. E., Seitzman, B. A., Nelson, S. M., Wig, G. S. & Gordon, E. M. Principles of
566 cortical areas and their implications for neuroimaging. *Neuron* **112**, 2837-2853 (2024).
567 53. Makin, T. R. & Krakauer, J. W. Against cortical reorganisation. *Elife* **12**, e84716 (2023).
568 54. Kolb, B. & Whishaw, I. Q. Mass Action and Equipotentiality Reconsidered. in *Brain Injury*
569 *and Recovery: Theoretical and Controversial Issues* (eds. Finger, S., Levere, T. E., Almli,
570 C. R. & Stein, D. G.) 103–116 (Springer US, Boston, MA, 1988).
571 55. Grimmelikhuijzen, C. J. & Westfall, J. A. The nervous systems of cnidarians. *EXS* **72**, 7–24
572 (1995).
573 56. Ricci, L. & Srivastava, M. Transgenesis in the acoel worm Hofstenia miamia. *Dev. Cell* **56**,
574 3160–3170.e4 (2021).
575 57. Breen, C. & Srivastava, M. A spreading, multi-tissue wound signal initiates whole-body
576 regeneration. *bioRxiv* 2024.12.10.627832 (2024) .
577 58. Baena, V., Schalek, R. L., Lichtman, J. W. & Terasaki, M. Serial-section electron
578 microscopy using automated tape-collecting ultramicrotome (ATUM). *Methods Cell Biol.*
579 **152**, 41–67 (2019).
580 59. Pachitariu, M., Rariden, M. & Stringer, C. Cellpose-SAM: superhuman generalization for
581 cellular segmentation. *bioRxiv* 2025.04.28.651001 (2025).
582 60. Pearson, B. J. *et al.* Formaldehyde-based whole-mount in situ hybridization method for
583 planarians. *Dev. Dyn.* **238**, 443–450 (2009).

61. Mathis, A. *et al.* DeepLabCut: markerless pose estimation of user-defined body parts with deep learning. *Nat. Neurosci.* **21**, 1281–1289 (2018).

62. Pereira, T. D. *et al.* SLEAP: A deep learning system for multi-animal pose tracking. *Nat. Methods* **19**, 486–495 (2022).

Acknowledgments

We thank Ugne Klibaite, Brandon Logeman, Aravinthan Samuel, David Palmer, Ishaan Chandok, Aditi Chandra, Benjamin de Bivort, Madeleine Snyder, Julian Smith III, and the entire Srivastava Lab for helpful discussion. We thank D. Marcela Bolanos, Samantha Tseng, and Julian Kimura for assisting with data collection, Maria Ericsson, Richard Schalek, Jeff Lichtman, and the Harvard Medical School Electron Microscopy Core Facility for enabling, advising and assisting on electron microscopy, Ed Soucy and Jazz Weisman for behavioral advice, and Tim Sackton and Tommy Tang for single-cell analysis advice. VC and APK are former and current Fellows of the Jane Coffin Childs Fund for Medical Research, respectively. VC acknowledges funding from the Harvard Brain Initiative's Postdoctoral Pioneer Award. AS was supported by a grant from the Harvard Museum of Comparative Zoology. This project was supported by an NIH BRAINI R34 award (1R34DA061984-01) to MS.

601 **Methods**
602
603 **Animal husbandry**
604 Juvenile *Hofstenia miamia* worms were reared in communal plastic tanks with artificial sea
605 water (37ppt, pH between 7.8 and 8.2), held at room temperature with an approximate day-light
606 cycle. Sea water was replaced twice weekly, and the worms were fed marine rotifers
607 (*Brachionus plicatilis*).
608
609 For behavioral experiments, worms were isolated from their culturing tanks, and placed in
610 individual wells of 6- or 12-well plates (Falcon #353046). Worms were typically 3-5 weeks post
611 hatching, at which point they varied in their sexual maturity. Preliminary observations indicated
612 that this variation did not affect foraging behavior, and each experiment was initiated with worms
613 from the same communal tank, of approximately the same age and size. Worms that were in the
614 middle stages of sexual maturity were fed rotifers, brine shrimp (*Artemia sp.*) or a mix of the two,
615 as previously described[33]. To amputate worms, we anesthetized them in 15% tricaine (ethyl 3-
616 aminobenzoate methanesulfonic acid; Sigma #E10521) for 10-20 minutes, and amputated them
617 with micro knives (Fine Science Tools #10316-14) before washing in artificial sea water to allow
618 recovery. Control worms in these experiments were anesthetized for the same amount of time,
619 but were not amputated. For foraging experiments, worms were starved for 1-2 weeks.
620
621 **Dyes and live imaging**
622 We used several live dyes to stain *H. miamia* brains. We used the voltage dye DiBAC4(3)
623 (Invitrogen #B438) to stain the nervous system. We dissolved DiBAC4(3) in pure ethanol to
624 create a 1mg/ml stock solution. We diluted this 1:1000 in artificial sea water with 15% tricaine.
625 Worms were incubated in this solution for 30 min. They were then mounted in a gel of 2%
626 methylcellulose (in artificial sea water containing 15% tricaine) on a glass slide, compressed
627 under a glass coverslip with clay feet, and imaged. The calcium dye ICR-1 AM (Ion Biosciences
628 #1091F) was reconstituted in DMSO and then diluted in artificial sea water with 15% tricaine to
629 a concentration of 40µM. Worms were incubated in this solution for 1-2hrs, then mounted on a
630 glass slide in methylcellulose, using the same procedure as above. SiR-Tubulin (Cytoskeleton,
631 CY-SC002) was dissolved in 50µL DMSO according to manufacturer instructions, then worms
632 were incubated in a 1:1000 solution in artificial sea water with 15% tricaine for 90m prior to
633 mounting as described above. *Troponin::Kaede* animals, described previously[56], were
634 anesthetized in tricaine, and mounted using the same procedures as above.
635
636 **Immunofluorescence**
637 We performed immunofluorescence using previously described protocols[33]. Briefly, worms were
638 fixed in 4% paraformaldehyde in artificial sea water for 1h at room temperature. Fixed animals
639 were washed in PBST (PBS + 0.1% Triton-X-100) three times, then blocked in 10% goat serum
640 (ThermoFisher, #16210072) in PBST for 1h at room temperature. Samples were incubated in
641 primary antibodies in blocking solution for 48h at 4°C, washed thoroughly (6x 20 minutes) in

642 PBST, incubated in blocking solution for 1h at room temperature, then incubated in secondary
643 antibody overnight at 4°C. Animals were washed thoroughly once more (6x 20 minutes) in
644 PBST, then counterstained with Hoechst 33342 and SiR-actin (where applicable). All steps were
645 carried out on an orbital shaker. Primary antibodies used: Par3 (St. John's Laboratory
646 #STJ94951, 1:200), pERK (Cell Signaling Technologies #4370T, 1:200) [57], FMRFamide
647 (EMDMillipore #AB15348, 1:1000)[29]. Counterstains used: Hoechst 33342 (ThermoFisher
648 #62249, 1:800) and SiR-actin (Cytoskeleton #CY-SC001, 1:1000)[39]. Goat anti-Rabbit IgG (H+L)
649 Cross-Adsorbed Secondary Antibody, Alexa Fluor™ 568 (ThermoFisher #A-11011, 1:800) was
650 used as a secondary antibody.
651
652 **Electron Microscopy**
653 We fixed hatchling juvenile worms using high-pressure fixation. A mix of intact worms and
654 amputated heads in 15% tricaine in artificial sea water were placed in 100μm-tall aluminium
655 planchettes, and were rapidly frozen in liquid nitrogen using a Leica EM ICE high-pressure
656 freezing instrument. These planchettes were then transferred under liquid nitrogen into cryovials
657 containing a freeze substitution cocktail (1% OsO4 and 0.1% uranyl acetate). Freeze
658 substitution involved holding the cryovials at -90°C for 36-48h, followed by warming up to -60°C
659 over 6h and holding for 6h, warming up to -30°C over 6h and holding for 3h, warming up to 0°C
660 over 6h and holding for 1h, and finally warming up to room temperature over 4h. Specimens
661 were then rinsed in acetone three times for 10m each. They were then extracted from the
662 planchettes and embedded in an Epon-Araldite resin. Resin blocks were baked at 60°C for 48h,
663 after which they were sectioned with a Leica UC6 ultramicrotome using a DiATOME diamond
664 knife, and collected onto tape using ATUM[58]. Sections of tape were then mounted on silicon
665 wafers as previously described[58], and were imaged using a Zeiss Sigma scanning electron
666 microscope. Neurites in Fig. 1i,j were segmented using Cellpose-SAM[59], with manual correction.
667
668 **Riboprobe synthesis and fluorescence *in situ* hybridization (FISH)**
669 We performed FISH using protocols described previously[25,60], with minor modifications. Briefly,
670 we used nested PCR to extract template sequences from cDNA. Riboprobes were synthesized
671 from these templates using a digoxigenin (DIG) labeling mix, as previously described[25,60].
672 Worms were starved for 1-2 weeks prior to fixation to ensure that their guts were empty. They
673 were then fixed in 4% paraformaldehyde in artificial sea water for one hour at room temperature.
674 We washed worms in PBST (PBS + 0.1% Triton-X-100), 50% PBST/50% MeOH solution, and
675 chilled MeOH for 5m each. They were then transferred to baskets in 24-well plates containing
676 800μL of solution per well, washed once in 50% MeOH/50% PBST, then twice in PBST. To
677 remove pigmentation and autofluorescence, they were bleached in a solution of 88.5% MilliQ
678 water, 4% hydrogen peroxide, 2.5% 20X SSC, and 5% formamide, then washed in PBST twice.
679 Worms were then incubated for 10 minutes in Proteinase K solution (0.1% SDS, 0.9% MilliQ
680 water, and 0.01% Proteinase K in PBST), post-fixed in formaldehyde solution (4% formaldehyde
681 in PBST) for 10m, and washed in PBST. They were then incubated in 50% PBST/50% PreHyb
682 (50% DI Formamide, 25% 20X SSC, 0.5% Tween-20, 24.5% MilliQ water, 0.001g/mL Yeast

RNA), transferred to 100% PreHyb and incubated at 56°C for 2hrs. 1μL of probe was then mixed with 799μL of hybridization solution (50% DI Formamide, 25% 20X SSC, 0.5% Tween-20, 5% dextran sulfate, 19.5% MilliQ water, 0.001g/mL Yeast RNA), denatured at 72°C for 5m, and distributed in the wells. The worms were moved into the probe solution, sealed, and incubated at 56°C overnight. The following day, the worms were washed twice in PreHyb, twice in 50% PreHyb/50% 2X SSCT (10% 20X SSC, 0.1% TritonX-100, 89.9% MilliQ water), 100% 2X SSCT, then 0.2X SSCT (1% 20X SSC, 0.1% TritonX-100, 98.9% MilliQ water), for 30m each at 56°C. They were then cooled at room temperature for 10mins, washed in PBST, incubated in blocking solution for 1hr (90% PBST, 5% horse serum, and 5% 10X Casein), then moved to 1:1500 blocking solution:Anti-DIG, sealed, and left at 4°C overnight. The next day they were washed six times for 20m each in PBST, incubated in tyramide buffer for 10m, then development solution (0.1% rhodamine, 0.1% IPBA, and 0.01% H2O2 in tyramide buffer) for 10m. They were then washed in PBST 3 times before being moved to a solution of 1:500 Hoechst 33342 (ThermoFisher #62249) in PBST, sealed, and left at 4°C overnight. Finally, they were washed in PBST, and then mounted on glass slides in VECTASHIELD® PLUS Antifade Mounting Medium (Vector Laboratories, H-1900). All steps except the 56°C incubations were carried out using an orbital shaker.

FISH analysis

We collected all images with a Leica SP8 point-scanning confocal microscope. 3D images of FISH-labeled neural markers in brains were generally acquired through a 20x objective. We then generated a maximum intensity z-projection of the brain for each of these images, and trained a supervised pixel classifier in ilastik to segment pixels that had FISH signal. These binary images were then smoothed in FIJI through a process of erosion and hole filling. We then segmented contiguous blobs containing fluorescent puncta, and filtered these to exclude blobs that contained fewer than 10 pixels – to remove noise that was sometimes captured by our segmentation.

To quantify regionalization of neural markers within the brain, we computed two indices of regionalization. First, we partitioned each brain into a heatmap containing 25 pixels, and we calculated the proportion of pixels occupied by fluorescent puncta. We calculated the Gini coefficient (a standard measure of inequality) of each heatmap. To correct for differences in regionalization expected as an artifact of sparseness, we simulated brains with uniformly distributed fluorescent puncta of the same sparseness. Computing the difference in Gini coefficients between real and matched, simulated brains provided a robust index of regionalization. Second, we fit a convex hull to fluorescent puncta in each brain, calculated the area occupied by this surface, and then calculated the ratio between this area and the area of the polygon encompassing the entire brain. To generate a second index of regionalization, we measured the difference between real ratios and corresponding ratios within simulated brains with uniformly distributed puncta.

724 **Behavior**

725 **Behavioral imaging**

726 All behavioral experiments were conducted in 6-well plates filmed with 850nm infrared side-
727 lighting from two LED strips behind a white acrylic diffuser (McMaster-Carr #8505K741), within a
728 custom behavioral chamber shielded from visible light. The chamber was cooled with a USB fan
729 to maintain temperatures between 22 and 25°C. Experiments were filmed in parallel using four
730 machine vision cameras (FLIR Blackfly BFS-U3-120S4M-CS and Basler Ace ac4024-29um
731 USB 3.0 monochrome, with Tamron M118FM16 16mm lenses) at 12 megapixels and 10Hz for
732 1h, streaming to a custom-built desktop computer; each video contained four or six wells of a
733 single plate within its field of view. We then used a custom MATLAB script for pre-processing:
734 background subtraction, contrast enhancement, and cropping the video into a set of separate
735 output videos for each well of the plate. We typically scaled videos to a resolution of 1000x1000
736 pixels, masking areas outside the arenas, and aligning their centers to make xy coordinates
737 comparable across videos.

738

739 **Immobilized rotifer foraging assay**

740 To study the foraging behavior of *H. miamia* presented with immobilized prey, we developed an
741 assay to present worms a choice between blocks of agarose that either did or did not contain
742 groups of live, immobilized rotifers. Rotifers were embedded in ~1% agarose blocks using the
743 following protocol. For each agarose block, 100μL of a well-mixed stock solution of rotifers (on
744 the order of thousands of rotifers per mL) or 100μL of artificial sea water for controls, was first
745 aliquoted into the bottom of a subset of wells of a 96-well plate. 100μL of hot 2% UltraPure Low
746 Melting Point agarose (Invitrogen #16520-100) was then added immediately above. The plate
747 was then cooled at 4°C for 30m. Each solid agarose block was then placed against the wall of a
748 well of a 6-well plate, with a block of agarose alone and a block of agarose containing rotifers at
749 opposite ends of the wall. A small volume of 2% agarose was then pipetted onto this block to
750 glue it to the wall of the plate. 5-10m later, 6ml of artificial sea water was pipetted into the well, a
751 single *H. miamia* worm was introduced to the well and the behavioral experiment initiated.

752

753 **Tracking and foraging analysis**

754 We trained custom models in DeepLabCut[61] and SLEAP[62] to track keypoints on the worm. To
755 study foraging behavior, we quantified the position and movement of worm centroids inferred
756 from these keypoints. We systematically excluded worms from the analysis if they were tracked
757 poorly, or which were inactive for sustained periods over the course of the experiment (a
758 minority of worms fit these exclusion criteria across our experiments, independent of their
759 feeding or amputation status). To quantify the proportion of time spent near food (i.e. rotifers
760 embedded in agarose), we defined an experiment-specific threshold distance, and quantified
761 the proportion of frames in which the worm was within that distance.

762

763 **Postural analysis**

For the datasets used for postural analysis, we tracked seven keypoints along the midline of the worm. We smoothed the xy coordinates of these points, used median-filling to remove NaNs, and then fit a 20-jointed spline to this data. We calculated the curvature of the spline as the normalized ratio of the sum of the lengths of its segments to the length between the first and last points. This ratio was scaled to lie within the range [-1,1], where -1 represented a sharp left bend, 0 represented the worm's posture when straight, and 1 represented a sharp right bend. Worm length was calculated as the sum of the segments composing the spline; this was z-scored to enable comparison across worms and across experiments in which the measured length varied slightly as a function of precise camera parameters. Speed was calculated as minimum displacement between splines in consecutive frames. All measures were smoothed and filtered again to remove outliers. We used PCA to reduce this curvature-length-speed space to 2D; we then used k-means clustering to partition this postural space into elemental postures as described in the text. Multiple large language models were used to assist with generating analysis code.

Single-cell RNA sequencing analysis

We integrated single-cell RNA sequencing libraries from three previous sequencing experiments. These included worms that ranged from hatchlings (i.e., juvenile worms that have just emerged from their egg shells) to adults, and worms in various stages of regeneration after a transverse amputation. We re-aligned these libraries to an updated *H. miamia* transcriptome[46]. We then regressed library identity to correct for batch effects, identified neural clusters, extracted and re-clustered neural cells.

Hunting behavior assay and analysis

To study the behavior of *H. miamia* actively hunting escaping prey, we introduced a single worm and a single brine shrimp to each well of a 6-well plate. We filmed these arenas for 1h at 10Hz in infrared lighting conditions, using the imaging parameters described above.

We then tracked worms and brine shrimp using custom-trained SLEAP models. To find the velocity of the worm at frame i while smoothing tracking noise, we averaged the center-of-mass velocity over five frames before and after frame i. The velocity correlation function was then calculated for the entire trajectory of each sample using the definition $\langle v_w(t+\Delta t) \cdot v_w(t)\rangle_t$, where $v_w(t)$ denotes the velocity of the worm at time t, and the average is taken over time t. The final velocity correlation function shown in Fig. S6d is obtained by averaging the velocity correlation functions of worms across different experiments with the same treatment.

To quantify the correlation between the velocity of the worm and the trajectory of the shrimp (Fig.4d,e; Fig. S6e), we used the smoothed worm velocity v_v and calculated its correlation with the vector connecting the worm's position to the shrimp's position in earlier frames. The correlation is defined as $\langle v_w(t) \cdot \Delta r_{v_{sh}}(t-\Delta t)\rangle_t$, where $\Delta r_{v_{sh}}(t-\Delta t)$ is the unit vector pointing from the worm at time t to the shrimp at time t-Δt.